Field-Induced Single Molecular Magnetism and Photoluminescence in Rare Cocrystals of Isomorphic Lanthanide(III) Coordination Compounds with Fully Substituted Pyridine-4-carboxamide Ligand

Balkaran Singh Sran, Sanyog Sharma, Fabrice Pointillart, Olivier Cador, Geeta Hundal

Field-induced Single Molecular Magnetism and Photoluminescence in Rare Cocrystals of Isomorphic Lanthanide (III) Coordination Compounds with Fully Substituted Pyridine-4-carboxamide Ligand.

Balkaran Singh Sran[a], Sanyog Sharma[a], Fabrice Pointillart*[b], Olivier Cador*[b] and Geeta Hundal*[a]

[a]Department of Chemistry, UGC Sponsored-Centre for Advanced Studies-II, Guru Nanak Dev University, Amritsar-143005, Punjab, India

[b]Univ Rennes, CNRS, ISCR (Institut des Sciences Chimiques de Rennes) - UMR 6226, 35000 Rennes, France

geetahundal@yahoo.com

Abstract: A series of four isomorphous, 1:2 (Complex :**L**) rare cocrystals of coordination compounds of Ln(III) ions as $[Ln(\mathbf{L})(NO_3)_3(H_2O)]_2[\mathbf{L}]_2$ (Ln(III) = Gd (**1**), Tb (**2**), Dy (**3**) and Ho (**4**)), were synthesized with N, N-diisobutylisonicotinamide (**L**) using metal-to-ligand ratio of 1:1. All compounds are dimeric in nature with two co-crystallised **L** molecules centro-symmetrically interspersed between two dimeric units with H bonded bridges between them to form interesting, self-assembled H-bonded tapes along the c axis. Detailed Shape analysis and Hirshfeld analysis are done to demonstrate geometry around the metal centres and various non-covalent interactions present in the systems, respectively. Magnetic studies show that compound **3** is a field-induced Single-Molecule Magnet (SMM) for which the magnetization relaxes through a combination of Orbach (Δ = 51 K and τ_0 = 3.1 $x10^{-7}$s) and Raman mechanisms. Solid state luminescence studies reveal that compounds **1, 2** and **3** are photoluminescent in the visible range while **4** exhibits luminescence in the NIR region. Compound **3** shows cold white light emission with CIE (International Commission on Illumination) coordinates (0.31, 0.30) and CCT (Correlated Color Temperature) value of 6942 K.

Introduction:

A high impetus area, in solid-state chemistry dealing with isolation and characterization of various crystal forms of a given molecule, includes phenomena like polymorphism, isomerism and co-crystallisation[1-11] which may impact the physicochemical properties and end up producing materials with improved performance in their applications.[12] Out of these three phenomena, co-crystallization entails the formation of a phase pure material composed of two or more compounds (molecular or ionic) in certain stoichiometric ratios, provided they are not simple salts or solvates[13] and intentionally playing with positions of molecules in their crystal lattice, aiming for better products than the parent compounds. Co-crystallisation in organic compounds is well known to give better pharmaceuticals, agrochemicals, explosives and pigments[14-20] while material chemistry has reported co-crystallized materials with enhanced magnetism, luminescence and mechanical strength.[21-24] Growth in organic co-crystals has been exponential owing to the similar crystallization kinetics and molecular structures of the components, connected through various non-covalent interactions.[25-26] However, such reports are rather limited in the case of coordination compounds[27-30] as different coordination modes of the precursor metal complexes result in different lattice packing forces and hence dissimilar crystallization kinetics. Lesser yet are the reports of co-crystals of a coordination complex of a ligand along with the free ligand. Gao *et al*., reported[31] two, multi-component cocrystals of coordination complexes of Cu(II) and Zn(II) with the corresponding uncoordinated neutral ligand and anions. However, such co-crystallization with Ln(III) as metal ions finds only one report so far [32] and is thus a very rare phenomenon, to the best of our knowledge and belief.

The interest in lanthanide (III) complexes for the past two decades emanates from their exceptional potential in the fields of luminescence and molecular magnets owing to their typical electronic structure. They are the most sought after metal ions in the pursuit of single-molecule magnets (SMM) due to their high spin values and magnetic anisotropy[33] while wide range intense, narrow and long-lived emission bands of their complexes more than qualify them as the new age luminescent materials. More recently the combination of these two properties to produce multifunctional opto-magnetic Ln(III) complexes is the new craze for research in this area.[34-46] For designing of photoluminescent SMM complexes the choice of the metal ion is the most crucial in terms of the kind of anisotropy in its electron density (prolate or oblate) followed by its emitting state and sensitizing mechanism. The latter depends wholly on the choice of ligand that could both sensitize the ion as well as

produce a ligand field further augmenting the anisotropy of the metal ion. The relevant literature shows that for opto-magnetic materials Dy(III) hits the charts followed by Yb(III), Tb(III) and Er(III) essentially in that order[47-48] due to its strong magnetic anisotropy[33] and possibility of white-light emission.[49-51]

In the present studies, we are reporting crystal structures of a series of four isomorphous and iso-structural coordination complexes $[Ln(\mathbf{L})(NO_3)_3(H_2O)]_2[\mathbf{L}]_2$ (Ln(III) = Gd (**1**), Tb (**2**), Dy (**3**) and Ho (**4**)), where **L** is N, N-diisobutylisonicotinamide (Scheme 1), all of which have crystallized as rare cases (*vide supra*) of 1:2 co-crystals of a dimeric complex unit and uncoordinated ligands **L**. The presence of both coordinated and co-crystallised free ligands creates a possibility of enhanced antenna effect, both 'through bond' and 'through space' sensitization mechanisms. The dimers and the free ligands are arranged in linear tapes, extending into H-bonded 2D networks. All the complexes have been studied for their magnetic and emission properties in the pursuit of opto-magnetic materials. **L** has evidently shown some antenna effect to produce sharp emission spectra for Dy(III) and Tb(III) and Ho(III) complex but not for Gd(III) complex where ligand-based emission dominates the spectrum. Dy(III) complex shows field-induced SMM behaviour with an effective barrier 51 K and also is a white light emitter with Commission Internationale de l'Eclairage (CIE) chromaticity coordinates 0.310, 0.300.

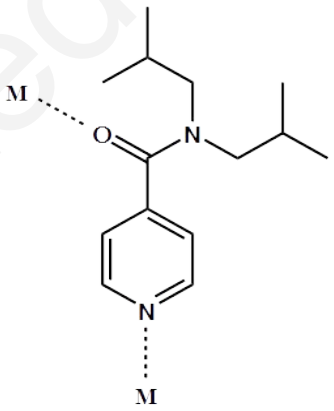

Scheme 1. Showing coordination mode of ligand (μ_2–κ^2, η^1:η^1)

Experimental section

Synthesis of N, N-diisobutylisonicotinamide (L): Preparation for N,N-diisobutylisonicotinamide is the same as reported earlier from our lab.[52]

Procedure for synthesis of complexes:

$[Gd(L)(NO_3)_3(H_2O)]_2[L]_2$ (1): $Gd(NO_3)_3 \cdot 6H_2O$ (68 mg, 0.2 mmol) in 20.0 mL of acetonitrile and ligand **(L)** (66mg, 0.2mmol) in 20.0 mL of methanol, were mixed together and refluxed with continuous stirring overnight, in a 50 mL round bottom flask. A clear solution was filtered out and its volume reduced to half by heating and then kept for slow evaporation. A viscous liquid appeared after a week. After 2 weeks crystals appeared in the viscous liquid. Crystals are separated from the liquid and washed with few drops of ice-cold methanol. Pale white block shaped crystals were obtained in 38% yield. IR (υ_{max}/cm^{-1}): 1595, 1281, 2967, Anal. Found: C, 40.36; H, 5.32; N, 11.17. Calc. for Complex **1**: C, 40.13; H, 5.15; N, 11.22%.

$[Tb(L)(NO_3)_3(H_2O)]_2[L]_2$ (2): Compound **2** was synthesized in a similar way to **1**, except that $Gd(NO_3)_3 \cdot 6H_2O$ was replaced by $Tb(NO_3)_3 \cdot 6H_2O$ (68 mg, 0.2 mmol). Pale white, block shaped crystals of **2** were obtained in 32% yield.IR (υ_{max}/cm^{-1}): 1595, 1284, 2974 .Anal. Found: C, 40.52; H, 5.59; N, 11.81. Calc. for Compound **2**: C, 40.32; H, 5.68; N, 11.63%.

$[Dy(L)(NO_3)_3(H_2O)]_2[L]_2$ (3): Compound **3** was synthesized in a similar way to **1**, except that $Gd(NO_3)_3 \cdot 6H_2O$ was replaced by $Dy(NO_3)_3 \cdot 6H_2O$ (86 mg, 0.2 mmol). Pale white, block shaped crystals of **3** were obtained in 31% yield. (IR (υ_{max}/cm^{-1}): 1591, 1277, 2964, Anal. Found: C, 40.44; H, 5.58; N, 11.79. Calc. for Compound **3**: C, 40.61; H, 5.51; N, 11.67%.

$[Ho(L)(NO_3)_3(H_2O)]_2[L]_2$ (4): Compound **4** was synthesized in a similar way to **1**, except that $Gd(NO_3)_3 \cdot 6H_2O$ was replaced by $Ho(NO_3)_3 \cdot 6H_2O$ (88 mg, 0.2 mmol). light orange, block shaped crystals of **4** were obtained in 36% yield. IR (υ_{max}/cm^{-1}): 1587, 1281, 2978, Anal. Found: C, 40.15; H, 5.54; N, 11.71. Calc. for Compound **4**: C, 40.35; H, 5.61; N, 11.93%.

Methods: Details about Instrumentation, X-ray data collection and structure solutions, Hirshfeld analysis, colour purity calculations can be found in the supporting information. A summary of the crystal data is given in Table 1.

Table 1. Crystallographic Data for compounds (**1-4**)

Identification code	**Compound 1**	**Compound 2**	**Compound 3**	**Compound 4**
Empirical formula	$C_{56}H_{92}Gd_2N_{14}O_{24}$	$C_{56}H_{92}Tb_2N_{14}O_{24}$	$C_{56}H_{92}Dy_2N_{14}O_{24}$	$C_{56}H_{92}Ho_2N_{14}O_{24}$
Formula weight	1659.93	1663.27	1670.43	1675.29
T(K)	150(2)	150(2)	150(2)	150(2)
Crystal system	Monoclinic	Monoclinic	Monoclinic	Monoclinic
Space group	*P 2₁/c*	*P 2₁/c*	*P 2₁/c*	*P 2₁/c*
Absorption coefficient (mm^{-1})	1.759	2.049	1.988	2.113
Crystal Size (mm^3)	0.22 x 0.18 x	0.19 x 0.16 x 0.12	0.18 x 0.16x 0.12	0.22 x 0.18 x 0.14
a (Å)	0.16	13.433(2)	13.785(2)	13.758(2)
b (Å)	13.926(5)	9.276(6)	9.5764(17)	9.5642(16)
c (Å)	9.559(3)	28.901(2)	29.667(5)	29.606(5)

α(°)	29.656(12)	90	90	90
β (°)	90	97.770(2)	97.893 (2)	97.948(4)
γ (°)	98.411(13)	90	90	90
V (Å^3)	90	3568(2)	3879.3(12)	3858.3(11)
Z	3905(2)	2	2	2
F(0 0 0)	2	1696	1700	1704
Reflections collected	1692	57916	22708	52001
Independent Reflections	64923	8602	7294	8582
Final R indices	9716	R1 = 0.0376	R1 = 0.0477	R1 = 0.0498
	R1 = 0.0668	wR2=0.0994	wR2=0.1092	wR2=0.1052
R indices (all data)	wR2=0.1287	R1 = 0.0473	R1 = 0.0772	R1 = 0.0898
	R1 = 0.1180	wR2=0.1048	wR2=0.1231	wR2=0.1176
λ(Å)	wR2=0.1463	0.71073	0.71073	0.71073
D_c(mg/m^3)	0.71073	1.548	1.430	1.442
Completeness to theta = 25.242^0	1.412	99.2%	98.9%	99.9%
Data / restraints / parameters	100%	8602 / 8 / 443	7294 / 9 / 439	8582 / 11 / 439
Goodness of fit on F^2	9716 / 9/ 439	1.002	1.085	0.909
CCDC No.	0.946	1976162	1976163	1976164
	1976161			

Result and Discussion

Crystal and molecular structure of compounds:

As all compounds are isomorphous and isostructural therefore the detailed description of only **1** has been given below and the molecular structures of (**2-4**) and their important bond distances and bond angles are given in the supplementary information (ESI, Table S1, Figure S1-S3).

[Gd(L)(NO$_3$)(H$_2$O)]$_2$[L$_2$](1): The asymmetric unit (ESI, Figure S4) of **1** shows a Gd(III) ion, coordinated by a bidentate, bridging ligand **L**, three nitrate ions, one water molecule and a non-coordinating **L** co-crystallized along with the complex. In the molecular structure of the dimeric compound **1** (Figure 1) Gadolinium centres are separated from one another by a distance equal to 8.458 Å. Both Gd(III) metal ions are nine-coordinated with the ligand having a μ^2–κ_2, η^1:η^1 mode (scheme 1) with Gd-N(Py), 2.611(4) Å and Gd-O(amide), 2.301(4) Å. Six positions around the metal ion are occupied by three bidentate chelating nitrate ions (av. Gd-O (nitrate) distance, 2.460 Å) and one remaining position is occupied by a water molecule (Gd-O, 2.344(5)Å). The arrangement around the metal centre leads to a coordination sphere with a spherical capped square antiprism (C_{4v}), symmetry. (The deviation from ideal symmetries has been determined by SHAPE analysis[53], ESI, Figure S5 Table S2).

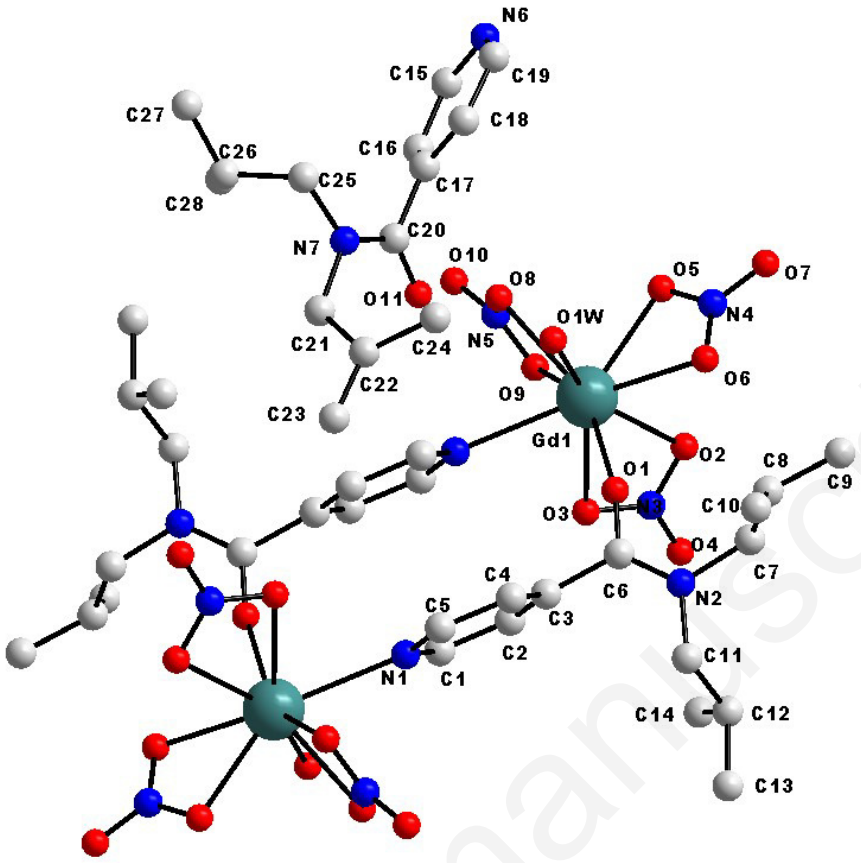

Figure 1. Showing the molecular structure of complex **1** along with the co-crystallized ligand.

The dihedral angles between the amide group and the pyridine ring are 75.48° and 61.52° for the coordinated and free **L**, respectively showing a rotation of 13.96° for the amide group in coordinating position. This, along with the dimeric nature of the complex allows strong π···π interactions between two pyridine rings in the dimer, with centroid···centroid 3.625 Å (ESI Figure S6). The d_{offset} distances and displacement angles were calculated as 1.48 Å and 24.09°. A unit cell packing for complex **1** is shown in ESI Figure S7. Two co-crystallised **L** molecules are centro-symmetrically interspersed between two successive dimeric units forming a bridge between them via H bonding through their N6 (pyridine) and O11 (amide) atoms (Figure 2). Each dimeric unit is involved in this H-bonding using its water molecule, O1W which acts as a double H-bond donor to N6 (Py) and O11 (amide) of the free **L** molecules, forming H-bonded tape along the *c* axis (Figure 2, Table S5 for H-bonding distances and symmetries). This tape is further supplemented by C-H...O interactions between nitrate group and methylene protons of the free ligands. Further, these tapes are extended to a 2D network in the *bc* plane as these dimeric units are connected to each other

by hydrogen bonding between oxygens of nitrate group and aromatic protons, down the *b* axis (C4−H4···O8,C4−H4···O10, Figure 3).

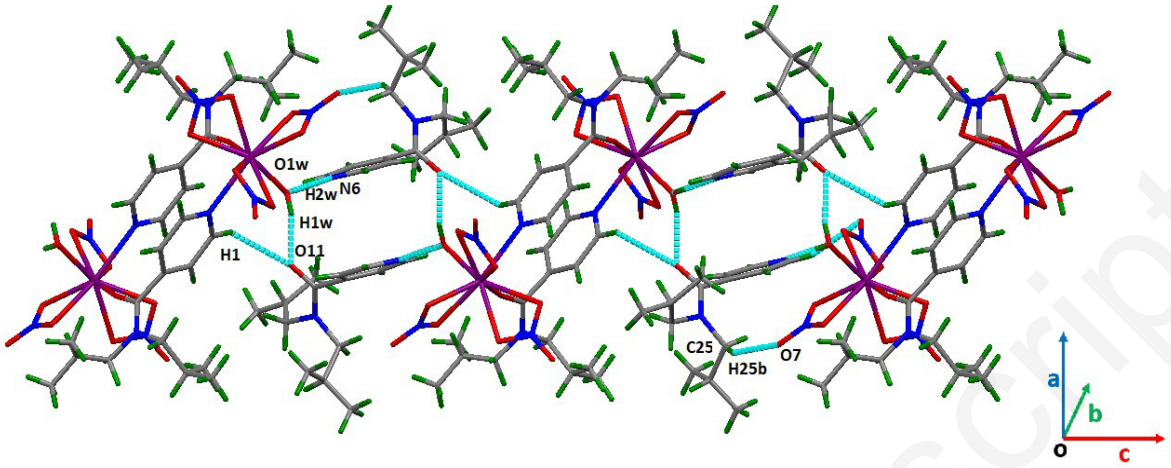

Figure 2. Showing the hydrogen bonding of the dimeric unit with cocrystallized ligand along the *c axis* forming 1D chains.

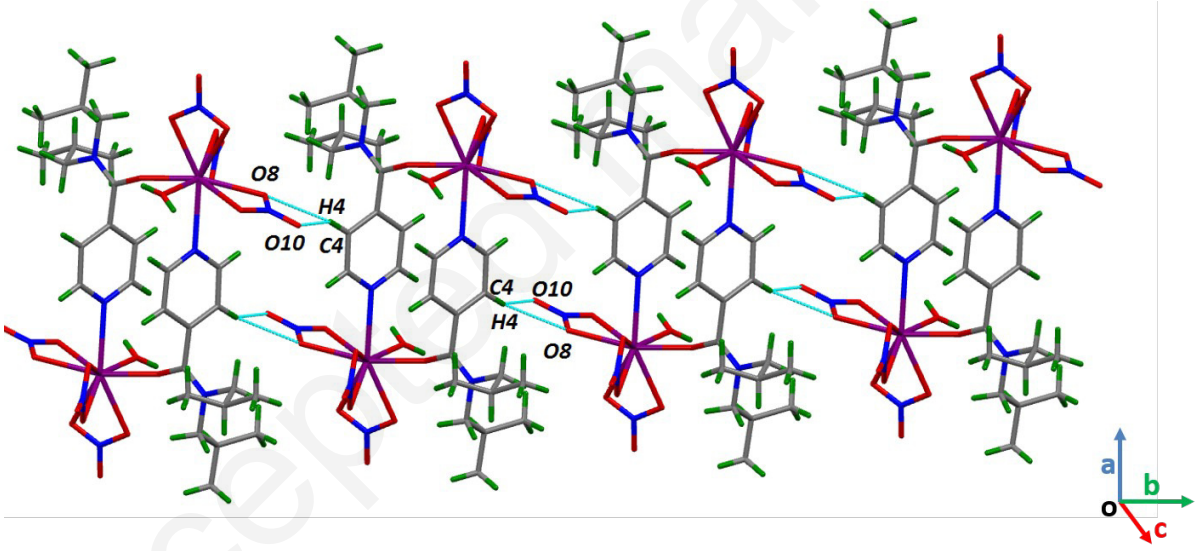

Figure 3. Showing the hydrogen bonding between dimeric units along *b* axis.

Figure 4a shows the self-assembly of two centrosymmetric, co-crystallized ligands between two dimers, along the *c* axis which gives a robust crystal structure. The absence of these co-crystallised **L** molecules generates voids between two dimeric units, which are being efficiently filled by these two **L** molecules (Figure 4b). These free **L** molecules seem to have stabilized the crystal structure in the ratio M:L 1:2 despite the fact that the reactions were run in the M:L ratio of 1:1.

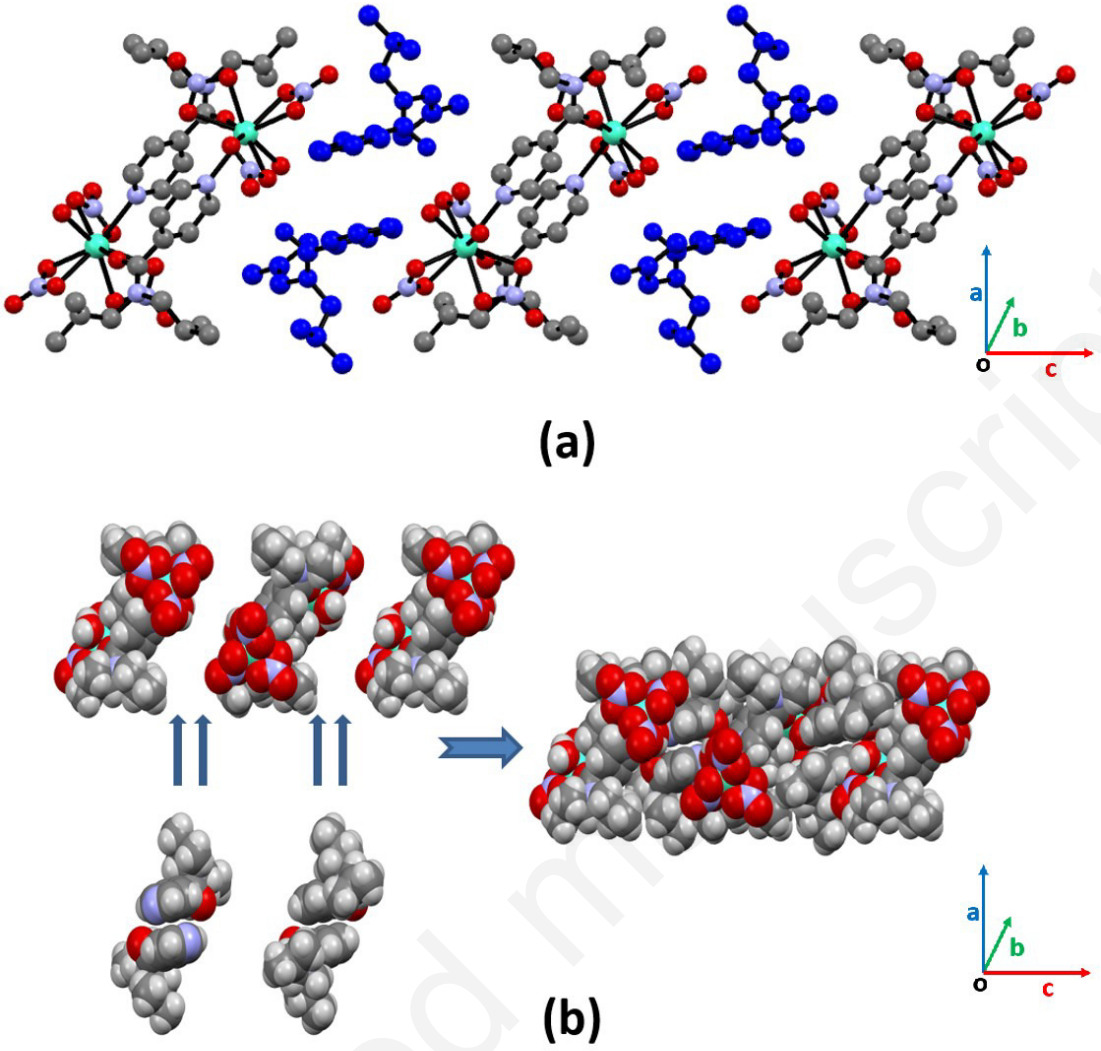

Figure 4. (a) Showing 1D representation of crystal packing along the *c* axis (cocrystalising **L** are shown in blue color (b) space-filling representation with and without free **L** along the *c* axis.

IR spectroscopy: Compound **1** shows a strong band at 1595 cm^{-1} which describes that amide oxygen is participating in coordination.[54-55]Presence of broad band for ν_{OH} at 3400 cm^{-1} in **1** shows coordinating water. The ν_{C-N}(amide) and ν_{C-H} stretching bands are assigned to 1476 cm^{-1} and 2979, cm^{-1}, for **1**. Three bands at 1423 cm^{-1}, 1281 cm^{-1} and 1016 cm^{-1} appear due to asymmetric NO_2, symmetric NO_2 and N-O stretching modes of coordinating nitrate group (FigureS7). [56] Similar bands have been observed for other compounds (**2-4)** and are given in the supplementary material (ESI, Figure S8-11, Table S3).

Thermogravimetric analysis

Thermogravimetric analysis was performed to check thermal stability of compounds (**1–4**) (Figure S1-S4). All complexes follow the same trend of decomposition, losing two coordinated water molecules up to 150 ^{o}C, endothermically. All **L** molecules (coordinating and free) are decomposed in the temperature range of 200–300°C, exothermally. Further they decomposition coordinating nitrates takes place up to 500^{o} C, leaving behind the metal skeleton residues after 700 ^{o}C. The detailed analysis for each compound is available in the ESI (Figure S12-S15).

Powder X-ray Diffraction studies

To confirm the phase purity of the bulk material correspond to the single crystal structure of complexes (**1-4**), the powder X-ray data were collected at room temperature. The experimental and simulated patterns show the phase purity of samples.(ESI, Figure S16-S19)

Hirshfeld analysis: To check the participation of various non-covalent interactions in the crystal structure, we performed the Hirshfeld surface analysis on all complexes, dividing the studies into three cases which differ in the part of the molecule considered as input for plotting Hirshfeld surface (HFS) i.e. case (I) the dimeric unit only, case (II) cocrystallized **L** only and case (III) both the dimer and the co-crystallized **L**. The results have been explained below for the complex **1** and are fully replicated by the remaining structures (**2-4**) as well (ESI, Figure S25-S27).

In case (I) d_{norm} surface shows that the dimeric unit is participating in the self-assembly employing H-bonding interactions through water molecules (red spots) (Figure 5a and ESI Figure S20) to N(pyridine) and O(amide) of the free **L** molecules. Similarly, this surface is connected with other dimeric units through hydrogen bonding from oxygens of nitrate group (color light red). In case(II), N(pyridine) and O(amide) from the free **L** are the potential interaction points (Figure 5b, red spots) which are connected via water molecules to two different dimeric units holding them perfectly in a linear tape (ESI, Figure S21).

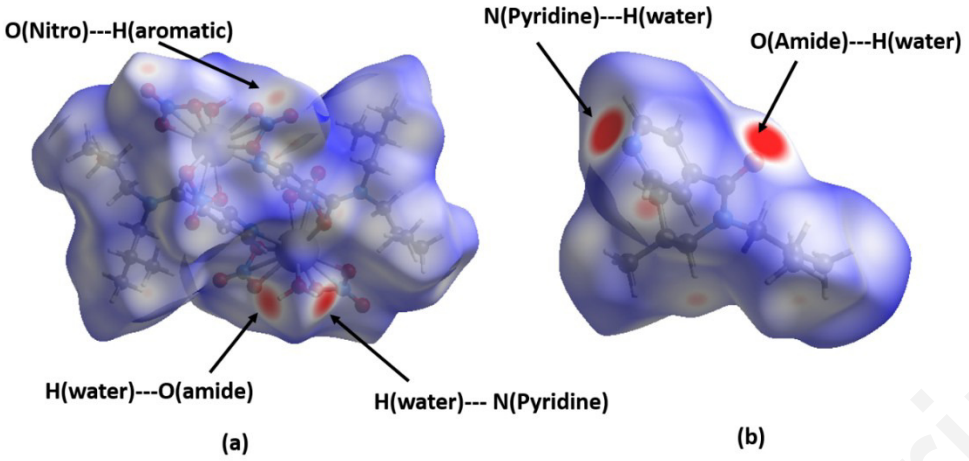

Figure 5. d_{norm} surfaces showing (a) Case I- O(Nitro)···H, H(water)···O(amide) and H(water)···N(pyridine) between the adjacent molecules for the dimeric unit (b) case II Showing the O(amide)···H, N(pyridine)···H interactions between the adjacent molecules for **L**. Red spots represent the strong point of interaction on the d_{norm} surface.

Comprehensive 2D fingerprints for all three cases are depicted in Figure 6 while the interaction- wise plots for each case are given in ESI (Figure S22-24). For case(I) (Figure 6a) of the dimeric unit shows a long and sharp spike and a short and blunt spike for O...H/H...O interactions, representing that it acts more of a H-bond donor (through water molecules) than a H-bond acceptor (through oxygens of nitrate groups). For case(II), **L** acts largely as H-bond acceptor for O...H/H...O interactions, due to N(pyridine)/O(amide) and weakly as H-bond donor through methylene protons therefore again an unsymmetrical pair of spikes is obtained (Figure 6b). Whereas the complete unit (case (III)) shows (Figure 6c) a pair of very symmetrical spikes due to a mutual balance in H-bond donation and acceptance between the successive units in the crystal structure.

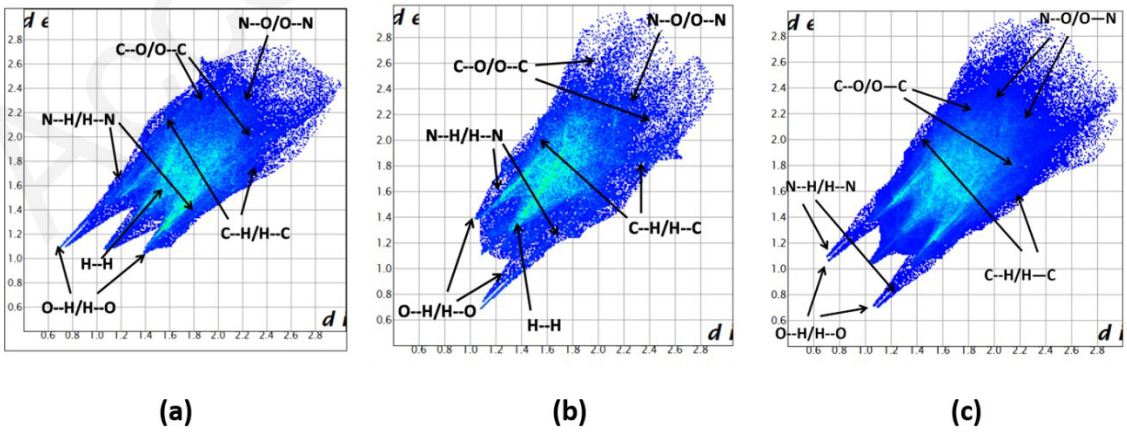

Figure 6. Showing 2D fingerprint plots for (a) case I (b) case II (c) case III

The quantitative participation (%) of each type of interaction, for all three cases in complexes **1-4** are shown in ESI, Figure S25-S27. These percentages are nearly equal for all complexes and also indicate that O...H/H...O H-bonding interactions are the most dominating ones after H…H interactions. These are followed by N(Py)...H except in case II where C...H are comparable to N...H for the obvious reason of being a HFS of the free **L** only.

Magnetic Properties

Static magnetic measurements: Static magnetic measurements were performed for all compounds (**1-4**) in temperature range 2-300K are shown in Figure 7. For compound **1** $\chi_M T$ is equal to 15.9 cm^3 K mol^{-1} at room temperature which is in good agreement with the expected value (15.8 cm^3 K mol^{-1}, $^8S_{7/2}$, $S = 7/2$, $L = 0$, $g = 2$) for two uncoupled Gd(III) ions.[57] Towards lower temperatures the value remains constant up to 20 K after which it decreases abruptly to 14.3 cm^3 K mol^{-1} at 2 K. For compound **2** $\chi_M T$ is equal to 23.5 cm^3 K mol^{-1} at room temperature which is in good agreement with the expected value (23.6 cm^3 K mol^{-1}, $^7F_6$, $S = 3$, $L = 3$, $J = 6$, $g = 3/2$) for two uncoupled Tb(III) ions. [57] On lowering the temperature it decreases steadily up to 100 K after which there is an abrupt decrease to a value of 16.9 cm^3 K mol^{-1} at 2 K.[57] For compound **3**, room temperature $\chi_M T$ is 28.2 cm^3 mol^{-1} K which is in good agreement with the expected value (28.3 cm^3 K mol^{-1}, $^6H_{15/2}$, $S = 5/2$, $L = 5$, $J = 15/2$, $g = 4/3$) for two uncoupled Dy(III) ions. $\chi_M T$ remains constant down to 150 K while cooling and then starts decreasing to a minimum of 17.3 cm^3 K mol^{-1} at 2 K. For compound **4,** $\chi_M T$ values are measured as 27.8 $cm^3 mol^{-1} K$ which is close to the expected value (28.1 cm^3 K mol^{-1}, $^5I_8$, $S = 2$, $L = 6$, $J = 8$, $g = 5/4$) for two isolated Ho (III) ions. [57] The compound also shows abrupt decrease below 100K and gives a value of 9.0 cm^3 K mol^{-1} at 2 K. For all the compounds, the decrease of the $\chi_M T$ can be attributed to the thermal depopulation of the m_J levels and intermolecular antiferromagnetic dipolar interaction while antiferromagnetic exchange interactions are excluded, analysing the exchange pathway between the spin carriers. At 2 K, the field dependence of the magnetization shows a classical behaviour with values at 50 kOe (ESI, Figure S28-31) far away from the expected saturation values in the multiplet ground state framework. This is due to the presence of magnetic anisotropy and/or low-lying excited states.[58]

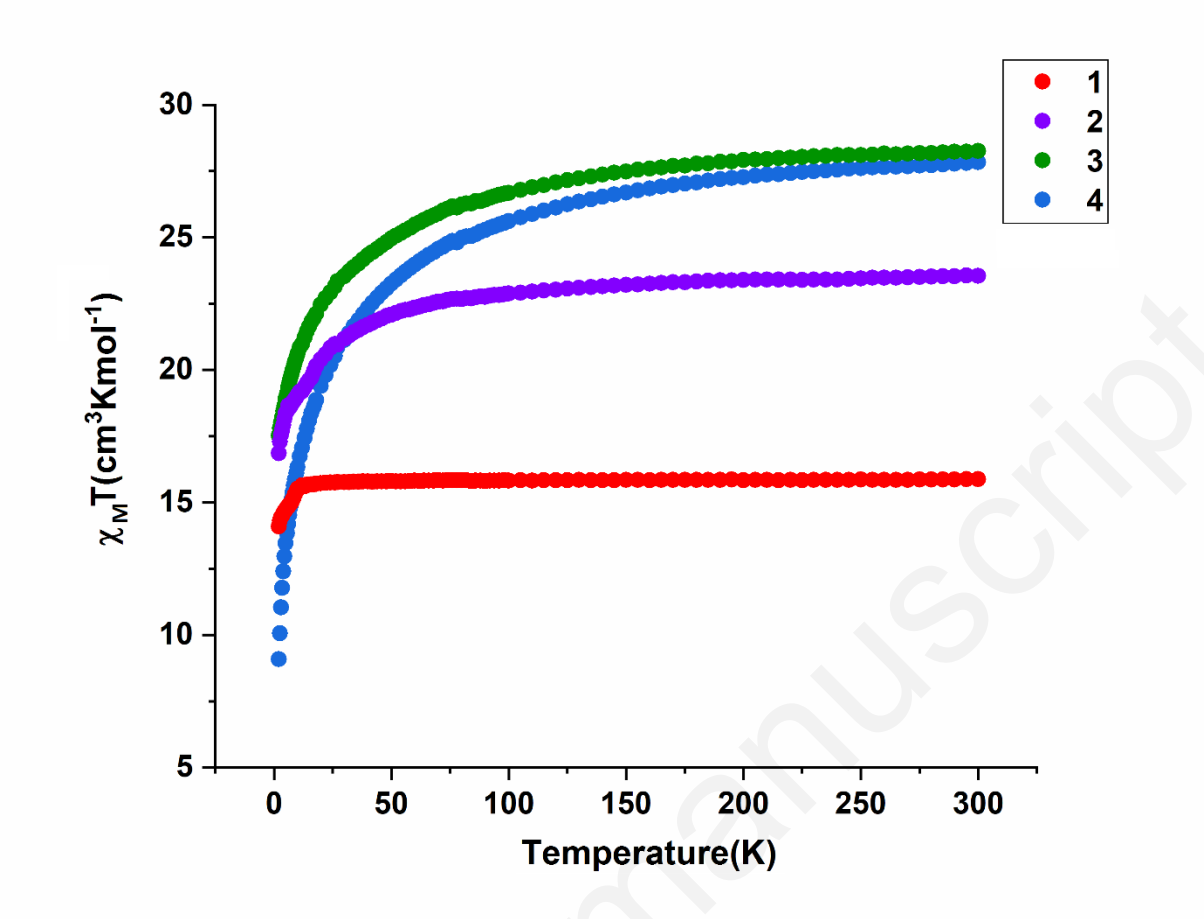

Figure 7. Showing thermal dependence of $\chi_M T$ for **1** (Red), **2** (purple), **3** (Green) and **4** (blue).

Dynamic magnetic measurements. None of the four compounds display out-of-phase, χ_M'', signal in zero external dc field and only **3** shows a non-zero χ_M'' when an external dc field is applied (ESI, Figure S32-S34). In case of **3**, an extended Debye model is used, [59-60] (see ESI) relaxation time (τ) has been calculated at fitting the frequency dependence of χ_M' (in-phase) and χ_M'' (out-of-phase) simultaneously at various applied dc field and plotted as log (τ) vs field. (See ESI, Figure S35). It is found that log (τ) values are almost constant from 1000-3000 Oe and from χ_M'' vs ν shows that at 2 kOe curve is better in shape. So dynamic magnetic measurements have been carried out at 2 kOe dc magnetic field for temperatures between 2 and 8 K for **3** (Figure 8). It shows a clear frequency dependence below 8 K with a maximum well visible in the range (1-1000 Hz) up to 6 K.

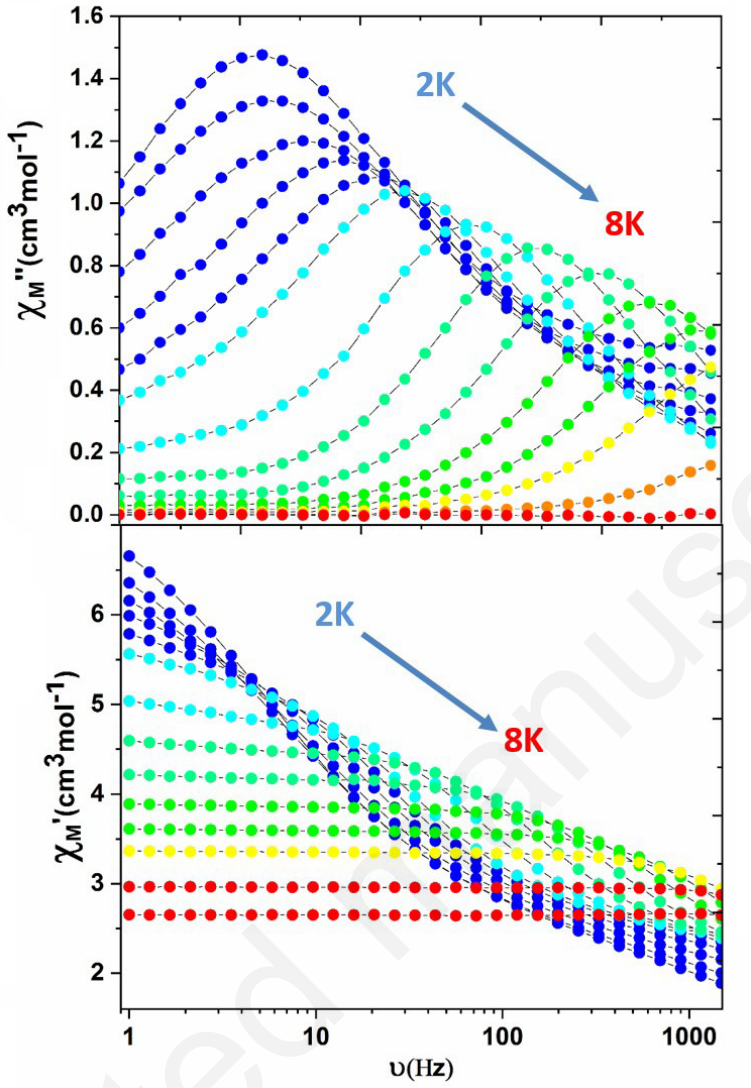

Figure 8. Frequency dependence of the out-of-phase (up) and in-phase (below) components of the ac magnetic susceptibility under applied field 2 kOe for compound **3**.

Using the extended Debye model, relaxation time (τ) has been calculated at fitting the frequency dependence of χ_M' (in-phase) and χ_M'' (out-of-phase) simultaneously at each temperature (see ESI, Figure S36-S39 Table S4,).[59-60] Relaxation time distribution parameter, α is large (0.33-0.52) in the low-temperature range (2-3.0 K) which suggests multiple relaxation processes occurring in this temperature range. This may be due to the presence of dipolar interactions in the lower temperature region.[61] Further, we fitted these relaxation times to the following equation 2 to find the relaxation pathway.

$$\tau^{-1}=\tau_0^{-1}\exp(-\Delta/T)+ CT^n \qquad \text{----------2}$$

From the data fitting it is found that best parameters are obtained by Raman + Orbach pathway (Figure 9) for compound **3** which gives us an activation energy barrier around 35.3(2) cm^{-1} (51 K) and relaxation time $3.1(1)x10^{-7}$s that falls well within the limit of a good SMM[67] in a temperature range of 2-6 K. Constant value obtained for Raman process is C=1.034(2) and n=4.92(2) (where C and n are the Raman constant and exponential, respectively) which is greater than 4 and falls in the expected criteria for Raman relaxation pathway.[63]

The absence of slow relaxation in compounds **2** and **4** can be explained on the basis of the fact that both of them (Tb(III) and Ho(III)) are non-Kramers ions. As it is well known that for a Kramers ion like Dy(III), there is always a bistable ground state, which has a necessary contribution to SMM behaviour, the lowest energy doublet has high $|M_J|$ and the complexity of the relaxation phenomena is related to the number of relaxation paths available. The latter could be anyone or all of the following i.e. reversal of magnetization in the lowest energy doublet via QTM, thermal mechanism via an excited state or quantum tunnelling of magnetization within an exciting doublet which is thermally activated. Comparing with Dy(III) ion, the Tb(III) and Ho(III) are non-Kramers ions, so their respective complexes will possess a bistable ground state only if they are presented in a highly axial symmetric ligand field.[64-65] As the coordination geometry is the same in all the complexes being reported here (*vide supra*) therefore the ligand field shows same amount of distortion from spherical symmetry. This distortion can support an oblate ion to accentuate its magnetic anisotropy, albeit to a limited extent (due to the donor atom at the capping position). Therefore all three complexes (**2-4**) of oblate ions should show SMM properties but the absence of any such behaviour for **2** and **4** may be due to them being non-Kramers ions, with crystal field not being sufficiently axial.

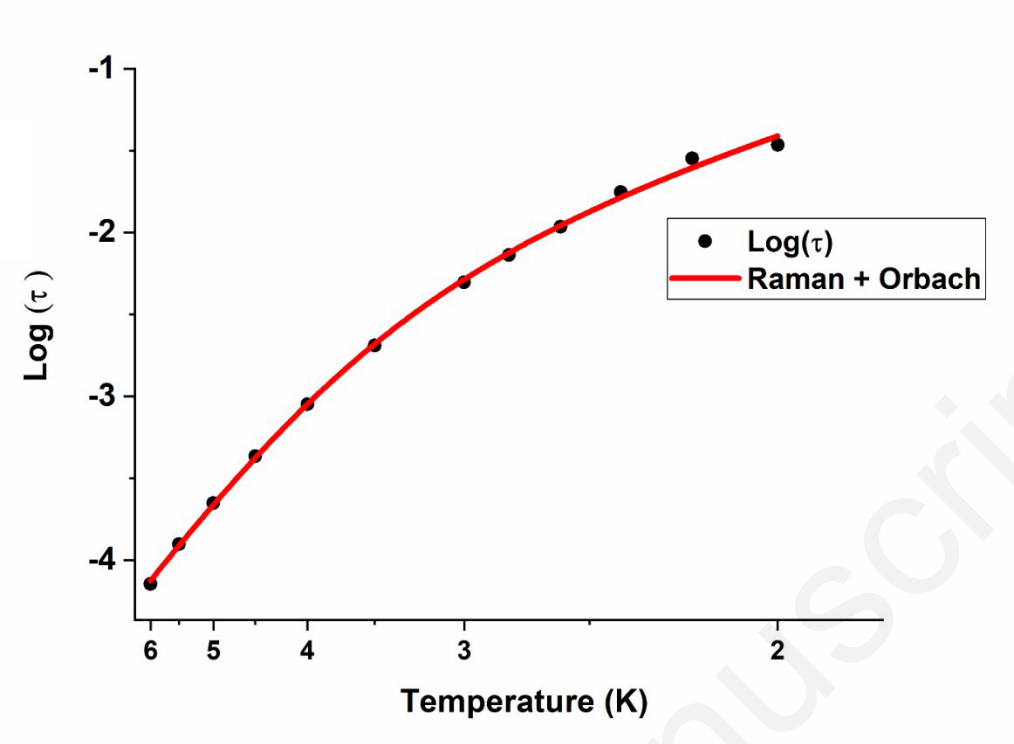

Figure 9. Temperature dependence of relaxation time log τ (black circles) with the best fitting curve (Red solid line) obtained by a combination of Raman and Orbach mechanisms with the parameters give in the text.

Photophysical Properties: Solid-state photophysical properties of compounds (**1-4**) are measured at room temperature. It is found that compounds **1-3** exhibit luminescence properties in the visible region and compound **4** exhibits luminescence properties in the NIR region. For Compound **1,** upon excitation at 382 nm, its emission spectrum gives broadband around 509 nm (19646 cm^{-1}) (Figure 10a), which has been assigned as an intra-ligand transition. This is done due to the fact that the free ligand (Figure S40, ESI) also shows a broad band in the same range. It is well known that for Gd(III) ion the energy gap between the ground state ($^8S_{7/2}$) and the excited state ($^6P_{7/2}$) is very large ≈ 32000 cm^{-1} which makes energy transfer impossible from the triplet state of ligand to the excited state of the metal ion.[66] For compound **2,** peaks are clearly visible at 489 nm (20449 cm^{-1}), 544 nm (18382 cm^{-1}), 583 nm (17152 cm^{-1}), 622 nm (16077 cm^{-1}) including less intense peaks at 650 nm (15384 cm^{-1}), 668 nm(14970 cm^{-1}), 679 nm (14727 cm^{-1}), upon excitation wavelength 365 nm (Figure 10b). These correspond to $^5D_4 \rightarrow {}^4F_6$, $^5D_4 \rightarrow {}^4F_5$, $^5D_4 \rightarrow {}^4F_4$, $^5D_4 \rightarrow {}^4F_3$ and less intense (Figure 10b (inset)) $^5D_4 \rightarrow {}^4F_2$, $^5D_4 \rightarrow {}^4F_1$, $^5D_4 \rightarrow {}^4F_0$. For compound **3,** excitation wavelength is 360 nm, which gives emission at 482 nm (20746 cm^{-1}), 573 nm (17452 cm^{-1}), 668 nm (14970

cm^{-1}), corresponding to $^4F_{9/2} \rightarrow {}^6H_{15/2}$(blue band), $^4F_{9/2} \rightarrow {}^6H_{13/2}$(Yellow band), $^4F_{9/2} \rightarrow {}^6H_{11/2}$(Red Band) (Figure 10c). Compound **4**, on excitation at 395 nm, shows emission at 970 nm (10309 cm^{-1}) in the NIR region corresponding to $^5F_5 \rightarrow {}^5I_7$ transitions (Figure 10d). Excitation spectra for compound **1-4** are given in ESI Figure S37.

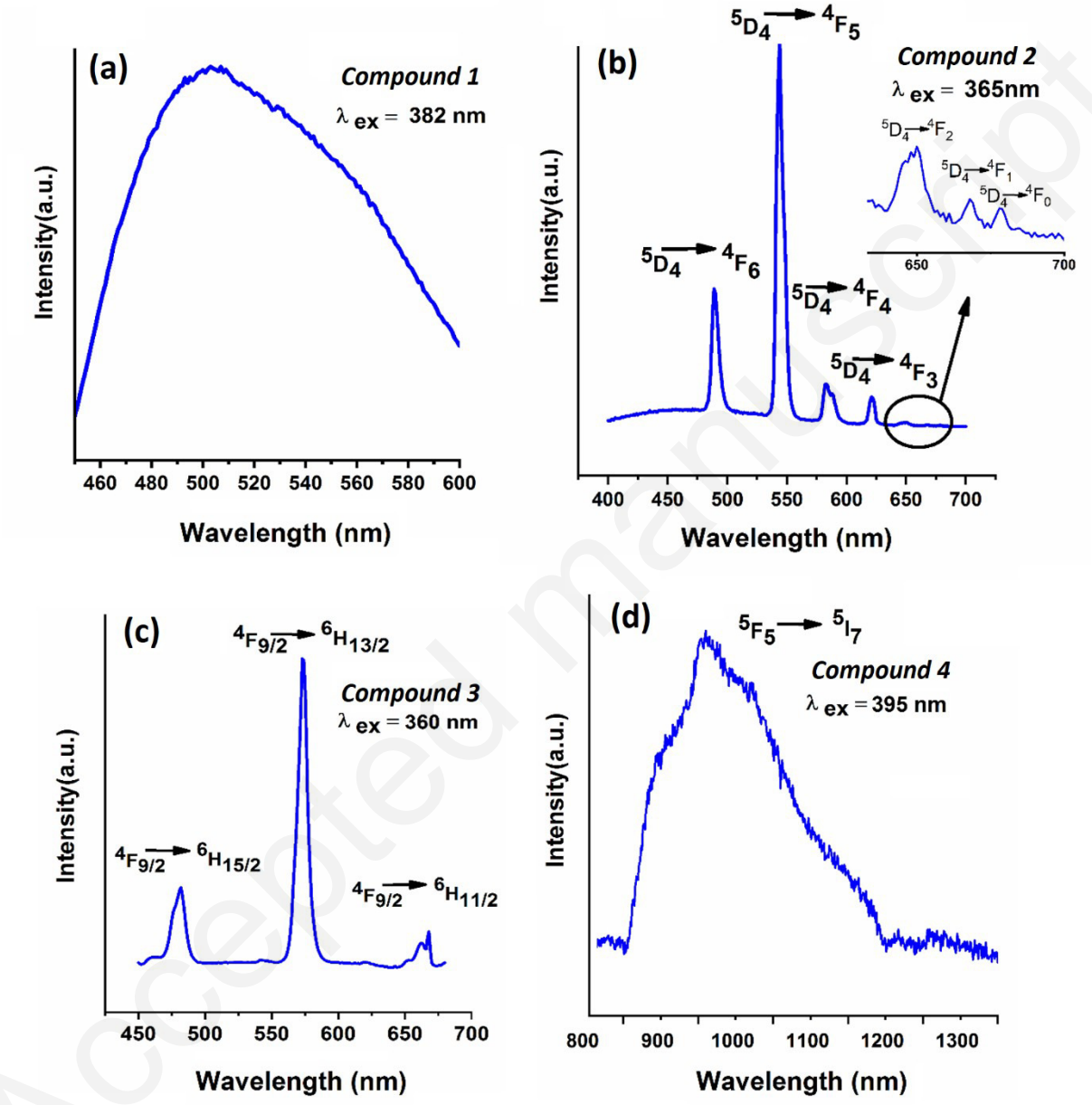

Figure 10. Room-temperature emission spectra of (a) **1** at λ_{em}(nm) = 509 (λ_{ex} = 382 nm) (b) **2** at λ_{em}(nm) = 489 , 544, 583, 622 , Inset- less intense peaks at 650 nm, 668 nm, 679 nm (λ_{ex} = 365 nm) (c) **3** at λ_{em}(nm) =482 , 573, 668 (λ_{ex} = 360 nm) (d) **4** at λ_{em}(nm) = 970 (λ_{ex} = 395 nm).

"Compound 2-4 show luminescence peaks as expected in compounds due to the successful energy transfer to the excited states of the lanthanides.[67] The excitation spectra (Figure S41) suggests that both antenna effect from the organic ligand and direct *f-f* excitations are involved in the sensitization mechanisms. From the luminescence data it is expected that triplet state energy of ligand **L** will lie (2500-4500 cm^{-1}) higher than the $^5D_4$ (20449 cm^{-1}), $^4F_{9/2}$ (20746 cm^{-1}) excitation state energies in Tb(III) and Dy(III), respectively and much lower than $^6P_{7/2}$ (32000 cm^{-1}) excitation level of Gd(III).[66] A schematic diagram representing the observed transitions and images for solid-state luminescence images under 365nm UV lamp for compound **1-3** are shown in Figure 11. Solid-state UV absorbance spectra for the ligand is shown in ESI Figure S42.

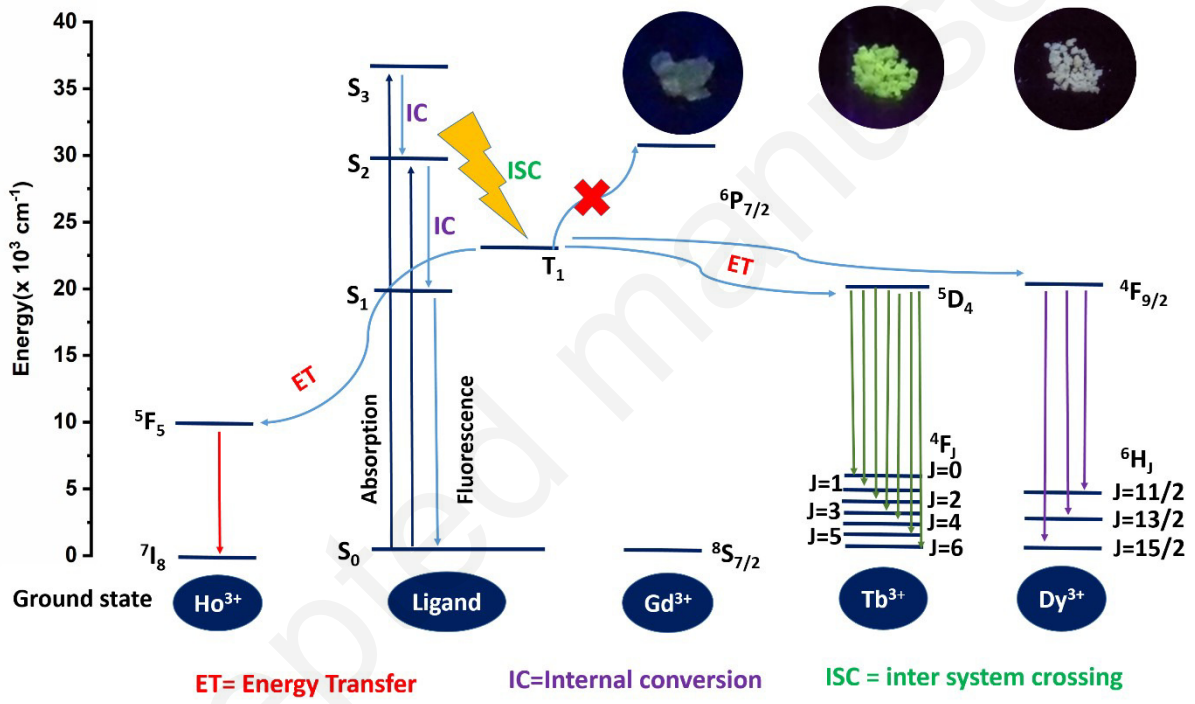

Figure 11. Schematic representation of energy level (Jablonski, Tailbones) diagram of the energy transfer process involved in the luminescence of compounds **1-4**. (Inset) Solid State luminescence for compounds **1-3** under 365nm UV lamp.

CIE Coordinates and CCT value calculations: The CIE chromaticity diagram (CIE 1931)[68] for **1-3** is shown in Figure 12. CCT (Correlated colour temperature) values are calculated by using the McCamy polynomial equation[69] (Equation 3) from the CIE co-ordinates(x,y) as following:

$$CCT = -449\,n^3 + 3525\,n^2 - 6823.3n + 5520 \qquad \text{-------3}$$

Where $n=(x-x_e)/(y-y_e)$ where x,y are chromacity coordinates and $x_e=0.332$, $y_e=0.186$ are the coordinates of chromaticity epicenter given by McCamy et. al.[69] CIE chromaticity coordinate values, CCT, and colour purities for Compounds **1-3** in the solid-state are given in Table 2.

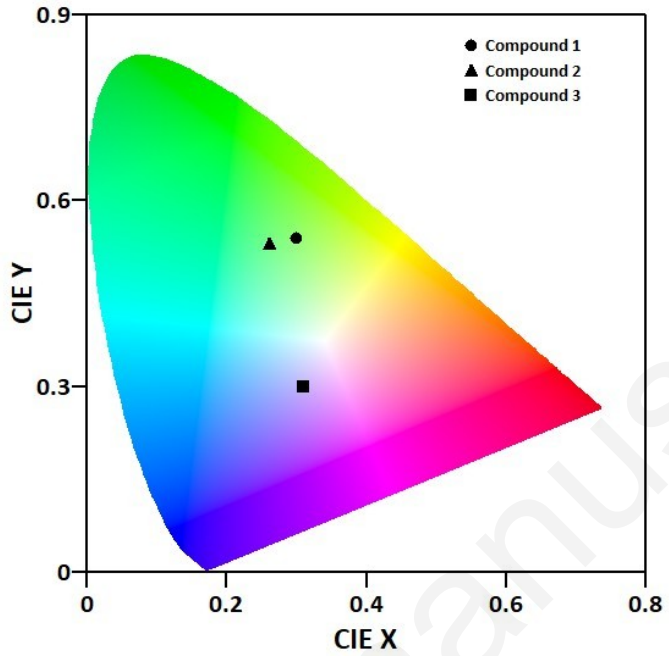

Figure 12. CIE chromaticity diagram (1931 CIE standard) for the compounds **1-3**.

It is found that for compound **3** CIE coordinates (0.31, 0.30) lie close to NTSC standard value for white light (0.310, 0.316).[70] Recent literature reports show that Dy(III) compounds are capable of producing white light as one component.[70] In terms of colour purity compound **3** displays very low colour purity which is essential for good white light emitter.[71]In general, the accepted CCT values should be greater than (> 5000 K) and (< 5000 K), for cold and warm light emission, respectively[72] The CCT value observed for **3** is 6942 K hence it may serve as a cold, white light emitter in lighting applications.[73]

Table 2: Representing CIE coordinates, CCT and % purities for compounds 1-3.

Compound	CIE x	CIE y	CCT	Purity %
1	0.30	0.54	6164	53.5
2	0.26	0.53	7021	41.8
3	0.31	0.30	6942	11.6

Conclusions

Four isomorphous and iso-structural complexes of **L** with Ln(III) having co-crystals with the free ligand **L** are being reported for the first time in the case of lanthanides. The self-assembly of two-component co-crystals is stabilized due to strong H-bonding interactions between them. Dynamic magnetic studies reveal that compound **3** is a field-induced SMM with an effective energy barrier around 51 K and with 3.1 x 10^{-7}s relaxation time. Complexes (**2-4**) display enhanced photoluminescence of the metal ions owing to the efficient antenna effect of the **L** organic chromophore while **1** shows only **L** centered luminescence. The Dy(III) complex exhibits good opto-magnetic properties and is a promising multi-functional material. The complex gives cold-white light emission with CIE coordinates (0.31, 0.30) and CRT value around 6942 K which can be used for light-emitting material. The synthetic strategy using co-crystallization approach might be an efficient approach to enhance both luminescent and magnetic properties by i) increasing the amount of organic ligand in the crystal lattice or/and allowing through bond and through space energy transfer to the lanthanide ion and ii) by playing the role of spacer to provide efficient magnetic isolation to the spin carriers.

Acknowledgement: BSS is thankful to UGC-BSR for a research fellowship and IFCPAR/CEFIPRA for Raman- Charpak fellowship, GH is thankful to CSIR (Research grant No. 01(2971)/19/EMR-II) for financial support. G.H. thanks the DST (Department of Science and Technology, India) for providing facilities under FIST and PURSE programs and the UGC (University Grants Commission) under CAS-II and UPE programs. SS is thankful to the CSIR for the fellowship of Research Associate. This work was supported by CNRS, Université de Rennes 1 and the European Commission through the ERC-CoG 725184 MULTIPROSMM (project n. 725184).

References

1. Bernstein, J. Polymorphism − A Perspective Cryst. Growth Des. **2011**, 11, 632−650.
2. Aakeroy, C. B.; Champness, N. R.; Janiak, C. Recent advances in crystal engineering. *CrystEngComm.* **2010**, 12, 22−43.
3. Bishop, R. Helical Tubuland Diols: A Synthetic and Crystal Engineering Quest *Acc. Chem. Res.* **2009**, 42, 67−78.

4. Nangia, A. Supramolecular chemistry and crystal engineering. *J. Chem. Sci*. **2010**, 122, 295−310.

5. Habgood, M.; Price, S. L. Isomers, Conformers, and Cocrystal Stoichiometry: Insights from the Crystal Energy Landscapes of Caffeine with the Hydroxybenzoic Acids. *Cryst. Growth Des.* **2010**, 10, 3263−3272.

6. Moulton, B.; Zaworotko, M. J. From Molecules to Crystal Engineering: Supramolecular Isomerism and Polymorphism in Network Solids. *Chem. Rev.* **2001**, 101, 1629−1658.

7. Desiraju, G. R. Crystal engineering: a holistic view. *Angew. Chem., Int. Ed*. **2007**, 46, 8342−8356.

8. Cruz-Cabeza, A. J.; Reutzel-Edens, S. M.; Bernstein, Facts and fictions about polymorphism. *J. Chem. Soc. Rev.* **2015**, 44, 8619−8635.

9. Stahly, G. P. Diversity in Single- and Multiple-Component Crystals. The Search for and Prevalence of Polymorphs and Cocrystals *Cryst. Growth Des.* **2007**, 7, 1007−1026.

10. Butterhof, C.; Barwinkel, K.; Senker, J.; Breu, J. Polymorphism in co-crystals: a metastable form of the ionic co-crystal 2 HBz·1 NaBz crystallised by flash evaporation *CrystEngComm.* **2012**, 14, 6744−6749.

11. Clarke, H. D.; Arora, K. K.; Bass, H.; Kavuru, P.; Ong, T. T.; Pujari, T.; Wojtas, L.; Zaworotko, M. J. Structure−Stability Relationships in Cocrystal Hydrates: Does the Promiscuity of Water Make Crystalline Hydrates the Nemesis of Crystal Engineering? *Cryst. Growth Des.* **2010**, 10, 2152−2167.

12. Karki, S.; Friščić, T.; Fabian, L.; Laity, P. R.; Day, G. M.; Jones, W. Improving Mechanical Properties of Crystalline Solids by Co-Crystal Formation: New Compressible Forms of Paracetamol. *Adv.Mater.* **2009**, 21, 3905−3909.

13. Aitipamula, S.; Banerjee, R.; Bansal, A. K.; Biradha, K.; Cheney, M. L.; Choudhury, A. R.; Desiraju, G. R.; Dikundwar, A. G.; Dubey, R.; Duggirala, M.; Ghogale, P. P.; Ghosh, S.; Goswami, P. K.; Goud, N. R.; Jetti, R. K. R.; Karpinski, P.; Kaushik, P.; Kumar, D.; Kumar, V.; Moulton, B.; Mukherjee, A.; Mukherjee, G.; Myerson, A. S.; Puri, V.; Ramanan, A.; Rajamannar, T.; Reddy, C. M.; RodriguezHornedo, N.; Rogers, R. D.; Row, T. N. G.; Sanphui, P.; Shan, N.; Shete,

G.; Singh, A.; Sun, C. C.; Swift, J. A.; Thaimattam, R.; Thakur, T. S; Thaper, R. K.; Thomas, S. P.; Tothadi, S.; Vangala, V. R.; Variankaval, N.; Vishweshwar, P.; Weyna, D. R.; Zaworotko, M. J. Polymorphs, Salts, and Cocrystals: What's in a Name? *Cryst. Growth Des,* **2012**, 12, 2147–2152.

14. Bolton, O.; Simke, L. R.; Pagoria, P. F.; Matzger, A. J. High Power Explosive with Good Sensitivity: A 2:1 Cocrystal of CL20: HMX. *Cryst. Growth Des.* **2012**, 12, 4311−4314.

15. Sekhon, B. S. Co-crystals of agrochemical actives. *International Journal of Agrochemicals and Plant Protection.* **2014**, 2, 44−47.

16. Bucar, D.-K.; Filip, S.; Arhangelskis, M.; Lloyd, G. O.; Jones, W.Advantages of mechanochemical cocrystallization in the solid-state chemistry of pigments: color-tuned fluorescein cocrystals. *CrystEngComm.* **2013**, 15 , 6289−6291.

17. Aitipamula, S.; Chow, P. S.; Tan, R. B. H. Trimorphs of a pharmaceutical cocrystal involving two active pharmaceutical ingredients: potential relevance to combination drugs. *CrystEngComm.* **2009**, 11, 1823−1827.

18. Aitipamula, S.; Wong, A. B. H.; Chow, P. S.; Tan, R. B. H. Pharmaceutical Salts of Haloperidol with Some Carboxylic Acids and Artificial Sweeteners: Hydrate Formation, Polymorphism, and Physicochemical Properties. *Cryst. Growth Des.* **2014**, 14, 2542−2556.

19. Banerjee, R.; Bhatt, P. M.; Ravindra, N. V.; Desiraju, G. R. Saccharin Salts of Active Pharmaceutical Ingredients, Their Crystal Structures, and Increased Water Solubilities. *Cryst. Growth Des.* **2005**, 5, 2299−2309.

20. Almarsson, Ö.; Zaworotko, M. J. Crystal Engineering of the Composition of Pharmaceutical Phases. Do Pharmaceutical Co- Crystals Represent a New Path to Improved Medicines? *Chem. Commun*. **2004**, 1889−1896.

21. Karki, S.; Friščić, T.; Fabian, L.; Laity, P. R.; Day, G. M.; Jones, W. Improving Mechanical Properties of Crystalline Solids by Co-Crystal Formation: New Compressible Forms of Paracetamol. *Adv. Mater.* **2009**, 21, 3905−3909.

22. Yan, D.; Delori, A.; Lloyd, G. O.; Friščić, T.; Day, G. M.; Jones, W.; Lu, J.; Wei, M.; Evans, D. G.; Duan, X. A Co-Crystal Strategy to Tune the Luminescent Properties of Stilbene-Type Organic Solid-State Materials. *Angew. Chem., Int. Ed.* **2011**, 50, 12483−12486.

23. Sonoda, Y.; Goto, M.; Tsuzuki, S.; Tamaoki, N. Fluorinated Diphenylpolyenes: Crystal Structures and Emission Properties. *J. Phys. Chem. A* **2007**, 111, 13441−13451.

24. Hori, A.; Takatani, S.; Miyamotoa, T. K.; Hasegawa, M. Luminescence from π-π Stacked Bipyridines through Arene−Perfluoroarene Interactions. *CrystEngComm* **2009**, 11, 567−569.

25. Allen, F. H. The Cambridge Structural Database: a Quarter of a Million Crystal Structures and Rising. *ActaCryst.* **2002**, B58, 380−388.

26. Devogelaer, J.-J.; Meekes, H.; Vlieg, E.; de Gelder, R. Cocrystals in the Cambridge Structural Database: a network approach, *ActaCryst.* **2019**, B75, 371-383

27. Wang, X. L.; Guo, Z. C.; Liu, G. C.; Qu, Y.; Yang, S.; Lin, H. Y.; Zhang, J. W. Tuning the Lead Complexes Based on a Double 1,10-Phenanthroline Derivative with Versatile Coordination BehaviorbyDicarboxylates: from 0D Nano-Ring to an Unprecedented 0D + 3DCocrystal. *CrystEngComm.* **2013**, 15, 551−559.

28. Mukherjee, P.; Drew, M. G. B.; Gomez-Garcia, C. J.; Ghosh, A.(Ni_2), (Ni_3), and (Ni_2 + Ni_3): A Unique Example of Isolated and Cocrystallized Ni_2 and Ni_3 Complexes. *Inorg. Chem.* **2009**, 48, 4817−4827.

29. Golbedaghi, R.; Salehzadeh, S.; Khavasi, H. R.; Blackman, A. G. Mn(II) Complexes of Three [2+2] Macrocyclic Schiff Base Ligands. Synthesis and X-ray Crystal Structure of the First Binuclear−binuclear Co-Crystal. *Polyhedron,* **2014**, 68, 151−156.

30. Evers, J. ; Gospodinov, I.; Joas, M.; Klapötke, T. M.; Stierstorfer, J.. Cocrystallization of Photosensitive Energetic Copper(II) PerchlorateComplexes with the Nitrogen-rich Ligand 1,2-Di(1H−tetrazol-5-yl)ethane. *Inorg. Chem*. **2014**, 53, 11749−11756.

31. Gao, X.-S.; Dai, H.J.; Tang, Y.; Ding, M.-J.; Pei, W.-B.; Ren, X.-M. Crystal Structures, Photoluminescence, and Magnetism of TwonNovel Transition-Metal Complex Cocrystals with Three-Dimensional H−Bonding Organic Framework or Alternating Noncovalent Anionic and Cationic Layers, *ACS Omega* **2019**, 4, 12230−12237.

32. Chen, Y.-C.; Liu, J.-L.; Lan, Y.; Zhong, Z.-Q.; Mansikkam-ki, A.; Ungur, L.; Li, Q.-W.; Jia, J.-H.; Chibotaru, L. F.; Han, J.-B.; Wernsdorfer, W.; Chen, X.-M.; Tong, M.-L. Dynamic Magnetic and Optical Insight into a High Performance Pentagonal Bipyramidal DyIII Single-Ion Magnet, *Chem. Eur. J.* **2017**, 23, 5708 – 5715.

33. Rinehart, J. D.; Long, J. R. Exploiting single-ion anisotropy in the design of f-element single-molecule magnets. *Chem. Sci.,* **2011**, 2, 2078–2085

34. Pointillart, F.; Cador, O.; Le Guennic, B.;. Ouahab, L. Uncommon lanthanide ions in purely 4*f* Single-Molecule Magnets . *Coord. Chem. Rev.* **2017**, *346*, 150-175.

35. Long, J.; Guari, Y.; Ferreira, R. A. S.; L. D. Carlos, Larionova, J. Recent advances in luminescent lanthanide based Single-Molecule Magnets. *Coord.Chem. Rev.* **2018**, 363, 57-70.

36. Wen, H.-R.; Zhang, J.-L.; Liang, F.-Y.; Yang, K.; Liu, S.-J.; Liu C.-M. Multifunctional Lanthanide Complexes Based on Tetraazacyclolamidophenol Ligand

with Field-Induced Slow Magnetic Relaxation, Luminescent and SHG Properties. *Eur. J. Inorg. Chem.* **2019**, 2019,1406–1412.

37. Brunet, G.; Marin, R.; Monks, M.-J.; Resch-Genger, U.; Galico, D. A.; Sigoli, F. A.; Suturina, E. A.; Hemmer, E.; Murugesu, M.; Exploring the dual functionality of an ytterbium complex for luminescence thermometry and slow magnetic relaxation. *Chem.Sci.* **2019**, 10, 6799-6868 .

38. Chen, W.-B.; Chen, Y.-C.; Liu, J.-L.; Jia, J.-H.; Wang, L.-F.; Li, Q.-W.;. Tong, M.-L A Piezochromic Dysprosium(III) Single-Molecule Magnet Based on an Aggregation-Induced-Emission-Active Tetraphenylethene Derivative Ligand. *Inorg. Chem.* **2017**, 56, 8730−8734.

39. Shintoyo, S.; Murakami, K.; Fujinami, T.; Matsumoto, N.; Mochida, N.; Ishida, T.; Sunatsuki, Y.; Watanabe, M.; Tsuchimoto, M.; Mrozinski, J.; Coletti, C.; N. Re, .Crystal Field Splitting of the Ground State of Terbium(III) and Dysprosium(III) Complexes with a Triimidazolyl Tripod Ligand and an Acetate Determined by Magnetic Analysis and Luminescence. *Inorg. Chem.* **2014**, 53, 10359−10369.

40. Errulat, D.; Marin, R.; Gálico, D. A.; Harriman K. L. M.,; Pialat, A.; Gabidullin B.; Iikawa, F.; Couto, O. D. D.; Moilanen, J. O.; Hemmer, E.; Sigoli, F. A.; Murugesu, M. A Luminescent Thermometer Exhibiting Slow Relaxation of the Magnetization: Toward Self-Monitored Building Blocks for Next-Generation Optomagnetic Devices. *ACS Cent.Sci.* **2019**, 5, 1187-1198

41. Ren, M.; Bao, S.-S.; Wang, B.-W.; Ferreira, R. A. S.; Zheng, L.-M.; Carlos, L. D. Lanthanide phosphonates with pseudo-D_{5h} local symmetry exhibiting magnetic and luminescence bifunctional properties. *Inorg. Chem. Front.,* **2015**, 2, 558–566.

42. Cucinotta, G.; Perfetti, M.; Luzon, J.; Etienne, M.; Car, P.-E.; Caneschi, A.; Calvez, G.; Bernot, K.; Sessoli, R.; Magnetic Anisotropy in a Dysprosium/DOTA Single-Molecule Magnet: Beyond Simple Magneto-Structural Correlations, *Angew. Chem. Int. Ed*.,**2012**, 51, 1606-1610.

43. Pointillart, F.; Le Guennic, B.; Cauchy, T.; Golhen, S.; Cador, O.; Maury, O.; Ouahab, L. A Series of Tetrathiafulvalene-Based Lanthanide Complexes Displaying Either Single-Molecule Magnet or Luminescence. Direct Magnetic and Photo-Physical Correlations in the Ytterbium Analogue. *Inorg. Chem*. **2013**, 52, 5978−5990.

44. Liu, T.-Q.; Yan, P.-F.; Luan, F.;. Li, Y.-X.; Sun, J.-W.; Chen, C.; Yang, F.; Chen, H.; Zou, X.-Y.; Li. G.-M. Near-IR Luminescence and Field-Induced Single Molecule Magnet of Four Salen-type Ytterbium Complexes. *Inorg. Chem.* **2015**, 54, 221−228.

45. Gálico, D. A.; Marin, R.; Brunet, G.; Errulat, D.; Hemmer, E.; Sigoli, F. A.; Moilanen , J. O.; Murugesu, M. Triplet-State Position and Crystal-Field Tuning in Opto-Magnetic Lanthanide Complexes: Two Sides of the Same Coin. *Chem. Eur. J.* **2019**, 25, 14625 – 14637.

46. Pointillart, F.; Jung, J.; Berraud-Pache, R.; Le Guennic, B.; Dorcet, V.; Golhen, S.; Cador, O.; Maury, O.; Guyot, Y.; Decurtins, S.; Liu, S. X.; Ouahab, L. Luminescence and Single-Molecule Magnet Behavior in Lanthanide Complexes Involving a Tetrathiafulvalene-Fused Dipyridophenazine Ligand. *Inorg. Chem.* **2015**, 54, 5384-5397.

47. Perfetti , M.; Pointillart , F.; Cador , O.; Sorace , L.;. Ouahab, L. Chapter 14: Luminescent Molecular Magnets, *Molecular Magnetic Materials: Concepts and Application,* Sieklucka, B., Pinkowicz, D., Eds.; WileyVCH: Weinheim, Germany, 2016.

48. Marin, R.; Brunet, G.; Murugesu, M. Shining new light on multifunctional lanthanide single-molecule magnets. Angew. Chem. Int. Ed. 10.1002/anie.201910299.

49. Chorazy, S.; Rams, M.; Nakabayashi, K.; Sieklucka, B.; Ohkoshi, S.-I. White Light Emissive Dy^{III} Single-Molecule Magnets Sensitized by Diamagnetic $[Co^{III}(CN)_6]^{3-}$ Linkers. *Chem. Eur. J.* **2016**, 22, 7371 – 7375.

50. Guo, P.-H.; Meng, Y.; Chen, Y.-C.; Li, Q.-W.; Wang, B.-Y.; Leng, J.-D.; Ding-Hua Bao,; Jia, J.-H.; Tong, M.-L. A zigzag Dy^{III}_4 cluster exhibiting single-molecule magnet, ferroelectric and white-light emitting properties. *J. Mater. Chem. C*, **2014**, 2, 8858–8864.

51. Wang, J.; Chorazy, S.; Nakabayashi, K.; Sieklucka, B.; Ohkoshi, S.-I. Achieving white light emission and increased magnetic anisotropy by transition metal substitution in functional materials based on dinuclear Dy^{III}(4-pyridone)[$M^{III}(CN)_6$]3- (M = Co, Rh) molecules. *J. Mater. Chem. C*, **2018,**6, 473-481

52. Pannu, A. P. S.; Kapoor, P.; Hundal, G.; Kapoor, R.,Corbella, M. ; Aliaga-Alcalde, N. ;Hundal, M.S. Magneto-structural studies of two new cobalt (ii)-N,N-diisobutylisonicotinamide compounds: $[CoLCl_2]n$ and $[Co(L)_2(H_2O)_4][CoLBr_3]_2 \cdot 2H_2O$ *Dalton Trans.* **2011**, 40, 12560−12569.

53. Llunell, M.; Casanova, D.; Cirera, J.; Alemany, P.; Alvarez, S. *SHAPE Program for the Stereochemical Analysis of Molecular Fragments by Means of Continuous Shape Measures and Associated Tools;* Departament de Quimica Fisica, Departament de Quimica Inorganica,and Institut de Quimica Teorica i Computacional - Universitat de ` Barcelona, Barcelona, Spain.

54. Lumb, I. ; Sran, B. S.; Sood, H. ; Arora, ; Hundal, G. Coordination chemistry of Cu(II), Co(II), Zn(II) and Ag(I) complexes of isomeric pyridine 2- and 4-carboxamides and their biological activity evaluation. *Polyhedron*, **2017,** 127, 153–166.

55. Nakamoto, K. *Infrared and Raman Spectra of Inorganic and Coordination Compounds*; 2nded; Wiley: New York, **1970**.

56. Gatehouse, B.M.; Livingstone, S.E.; Nyholm, R.S. Infrared Spectra of Some Nitrato-co-ordination Complexes. *J. Chem. Soc. ,***1957,** 4222-4225.

57. Kahn, O. *Molecular Magnetism,* VCH, New York, **1993.**

58. Jeletic, M.; Lin, P.-H.; Roy, J. J. L.; Korobkov, I.; Gorelsky, S. I.;. Murugesu, M An Organometallic Sandwich Lanthanide Single-Ion Magnet with an Unusual Multiple Relaxation Mechanism. *J. Am. Chem. Soc*., **2011,** 133**,** 19286-19289.

59. Dekker, C.; Arts, A. F. M.; Wijn, H. W.; van Duyneveldt, A. J.; Mydosh, J. A. Activated dynamics in a two-dimensional Ising spin glass: $Rb_2Cu_1-xCo_xF_4$. *Phys. Rev. B,* 40, **1989**, 11243–11251.

60. Cole, K. S.; Cole, R. H; Dispersion and Absorption in Dielectrics I. Alternating Current Characteristics. *J. Chem. Phys.,* **1941**, **9**, 341–351

61. Morita, T.; Katoh, K.; Breedlove, B. K.; Yamashita, M. Controlling the Dipole−Dipole Interactions between Terbium(III) Phthalocyaninato Triple-Decker

Moieties through Spatial Control Using a Fused Phthalocyaninato Ligand. *Inorg. Chem.* **2013**, 52, 13555−13561

62. Shen, H.-Y.; Wang, W.-M.; Gao, H.-L.; Cui, J.-Z. Near-infrared luminescence and SMM behaviors of a family of dinuclear lanthanide 8-quinolinolate complexes. *RSC Adv.,* **2016**, 6, 34165–34174.

63. Zadrozny, J. M.; Atanasov, M.; Bryan, A. M.; Lin, C.-Yi; Rekken, B. D.;. Power, P. P; Neese, F.; Long, J. R.; Slow magnetization dynamics in a series of two coordinate iron(II) complexes. *Chem. Sci.,* **2013**, 4, 125–138.

64. Mandal, L.; Biswas, S.; Cosquer, G.; Shen , Y.; Yamashita, M. Anion-driven structures and SMM behavior of dinuclear terbium and ytterbium complexes. *Dalton Trans.* **2018**, 47, 17493−17499.

65. Harriman, K.L.M.; Errulat, D.; Murugesu, M.; Magnetic Axiality: Design Principles from Molecules to Materials.*Trends chem.* **2019***,* 1,425-439.

66. Jiménez, J. A. Silicon-induced UV Transparency in Phosphate Glasses and its Application to the Enhancement of the UV Type B Emission of Gd^{3+}. *ACS Appl. Mater. Interfaces,* **2017,** 9, 15599-15604.

67. Jia, J.-H.; Li, Q.-W.; Chen, Y.-C.; Liu, J.-L.; Tong, M.-L. Luminescent single-molecule magnets based on lanthanides: Design strategies, recent advances and magneto-luminescent studies. *Coordination Chemistry Reviews*, **2019**, 378, 365–381.

68. Wyman, C.; Sloan, P.-P.; Shirley, P. Simple Analytic Approximations to the CIE XYZ Color Matching Functions. *J. Comput. Graph. Technol.* **2013**, 2, 1−11.

69. McCamy, C. S. Correlated Color Temperature as an Explicit Function of Chromaticity Coordinates. *Color Res. Appl.* **1992**, 17,142−144.

70. Manzur, J.; Costa de Santana, R.; Maia, L. J. Q. ; Spodine, A. V. E. Tuning White Light Emission in Dinuclear Phenoxo Bridged Dy(III) Complexes *Inorg. Chem.* **2019,** 58, 10012−10018.

71. Alexander, D.; Thomas, K.; Gopinath, R.J. M.; Joy , M.; Biju, P.R. ; Unnikrishnan, N.V.; Joseph, C. Novel white light emitting dysprosium oxalate nanocrystals: Competing luminescence quenching by the features of Dy-Oxalate layered structure *Journal of Alloys and Compounds ,* **2019** , 804 252-261.

72. Singh, D. K.; Manam, J. Investigation of structural, spectral and photometric properties of $CaTiO_3:Dy^{3+}$ nanophosphors for the lighting applications *Electron. Mater. Lett.*, **2017**, 4, 292-301.

73. Adhikari, G. C.; Thapa, S.; Zhu, H.; Grigoriev, A.; Zhu, P. Synthesis of $CsPbBr_3$ and Transformation into Cs_4PbBr_6 Crystals for White Light Emission with High CRI and Tunable CCT. *J. Phys. Chem. C.* **2019**, 123, 12023−12028.

For TOC only

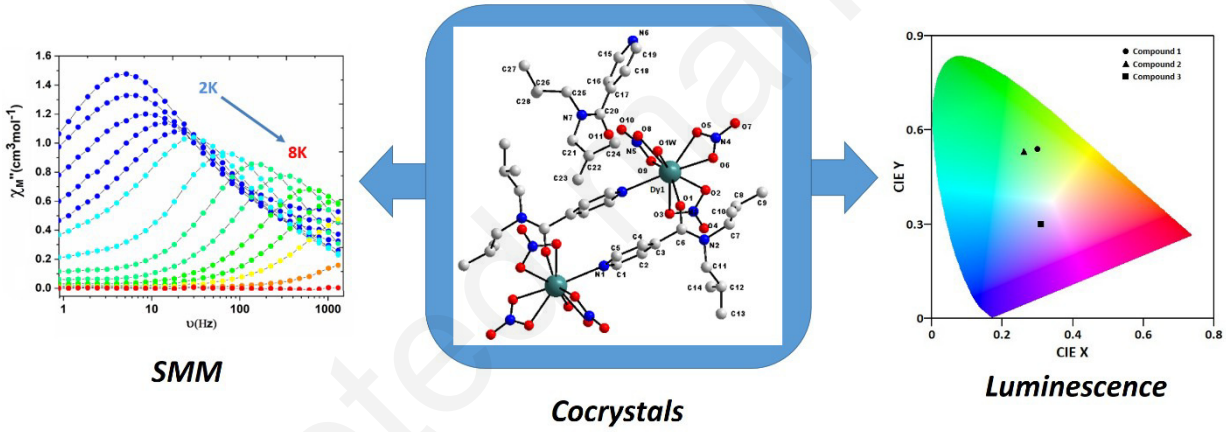

A series of four isomorphous, 1:2 (Complex :**L**) cocrystals of dimeric coordination compounds of Ln(III) ions as $[Ln(\mathbf{L})(NO_3)_3(H_2O)]_2[\mathbf{L}]_2$ (Ln(III) = Gd (**1**), Tb (**2**), Dy (**3**) and Ho (**4**)), were synthesized with N, N-diisobutylisonicotinamide (**L**) along with two co-crystallised **L** molecules centrosymmetrically. Compound **3** turns out to be a promising opto-magnetic material by being a field-induced Single-Molecule Magnet (SMM) (Δ = 51 K) and shows cold white light emission with CCT value of 6942 K.